The intrinsic error of exposure fusion for HDR imaging, and a way to reduce it

Raquel Gil Rodríguez
raquel.gil(at)upf.edu
Javier Vazquez-Corral
javier.vazquez(at)upf.edu
Marcelo Bertalmío
marcelo.bertalmio(at)upf.edu

Department of Information and Communication Technologies
Universitat Pompeu Fabra
Barcelona, Spain

Abstract

In this paper we present a novel approach to the problem of exposure fusion of a stack of pictures for the generation of high dynamic range (HDR) radiance maps. All exposure fusion approaches, when applied on 8-bit non-RAW pictures, perform photometric calibration by estimating and inverting the camera response function, which is assumed to be a channelwise-independent function which does not change with the exposure. Our experiments show that these assumptions do not always hold and that the camera may automatically introduce changes (in gain, white balance, gamma correction value) from one exposure to the next when performing the non-linear operations involved in recording pictures in non-RAW formats such as JPEG. The net result is that HDR radiance maps obtained from exposure fusion of non-linear data may have substantially more error than if computed directly from the linear, RAW data. Our proposed method overcomes this problem and compensates for the changes introduced by the camera by matching the color correction and gamma correction transforms of all pictures to those of a reference picture in the stack, providing a clear improvement in terms of PSNR with respect to the classical method of Debevec and Malik.

1 Introduction

Natural scenes commonly present a wide dynamic range, and the human visual system is able to capture subtle details in both dark and bright areas. This is not the case for standard digital cameras, which are limited in the dynamic range they are able to represent. The 12-bit or 14-bit values captured at sensor level and which are proportional to light intensity (this is the *linear* data, stored in RAW format) go through a chain of color-correction transformations culminating in a non-linear transform (gamma correction) followed by quantization in 8 bits per channel. The net result is that standard cameras are only able to capture different intervals of the luminance range at different exposure times, in particular, bright areas are captured at short exposure times, while dark areas are captured at longer exposure times.

To overcome this limitation, Mann and Picard [16] presented the idea of creating a high dynamic range (HDR) radiance map (an image with values that are proportional to the scene radiance at each point) by performing exposure fusion of a set of low dynamic range (LDR)

images. There is a vast literature on HDR imaging, see [17, 21] and references therein. While most methods for exposure fusion assume that both the camera and the scene are static [5, 16, 18, 23], there are also many works contemplating camera and/or object motion [8, 10, 11, 15], and some for video as well [9, 12, 22]. Exposure fusion approaches assume the following image formation model:

$$J(p) = f\left(E(p)\Delta t\right), \tag{1}$$

where Δt is the exposure time, p is a pixel location, $E(p)$ is the scene radiance value at p, f is a non-linear transform usually denoted as the camera response function (CRF), and finally $J(p)$ is the stored 8-bit image value, corresponding to one color channel. Analogous expressions hold for each of the three color channels, for which the function f might be different. In a static scene the values $E(p)$ remain constant, so taking a stack of N pictures by varying the exposure times gives us for each image

$$J_i(p) = f\left(E(p)\Delta t_i\right), \;\; i = 1, \ldots, N, \tag{2}$$

where the subindex i denotes the different exposures *and it is also assumed that the function f remains constant as Δt_i changes*. Exposure fusion methods estimate the inverse g of the CRF f, $g \equiv f^{-1}$, apply it to the image values $J_i(p)$ and then divide by the exposure time Δt_i so as to obtain one estimate of $E(p)$ for each image i in the stack:

$$\frac{g(J_i(p))}{\Delta t_i} = E(p), \;\; g \equiv f^{-1}. \tag{3}$$

These N estimates of $E(p)$ are then averaged in order to provide the final output, the HDR radiance value for pixel p.

We can see then how all exposure fusion approaches share a set of building assumptions for the camera capture:

1. Different color channels are independent.
2. In-camera non-linear correction curves are monotonic and smooth, but arbitrary in shape[1].
3. The camera response remains constant while changing the exposure.

These three assumptions, which made sense for film photography, are not an accurate model of how digital cameras work. Digital cameras follow a typical camera color processing pipeline [3] that can be expressed as

$$\begin{bmatrix} R \\ G \\ B \end{bmatrix}_{out} = \left(\alpha \cdot A \cdot \begin{bmatrix} R \\ G \\ B \end{bmatrix}_{in} \right)^{\gamma}, \tag{4}$$

where $[R,\ G,\ B]_{in}$ is the sensor raw triplet (usually in 12 or 14 bits) and it is linearly related to the scene radiance, $[R,\ G,\ B]_{out}$ is the pixel value at the end of the pipeline (in 8 bits per channel), A is a 3×3 matrix that combines the different color channels taking into account white-balance, color encoding and color characterization, α is a gain value, and γ is a value,

[1] Although some models, like [16] are more restrictive and others, like [5], more general.

typically between $1/1.8$ and $1/3$, performing gamma correction (notice that we omit demosaicing, denoising, compression, etc: for a complete explanation of these pipeline processes see [2]). The implications, for the above assumptions, of using this more realistic model are the following:

1. The three channels R, G, B are not independent, because the matrix A is not diagonal as it incorporates color processing steps like color characterization [26] aside from white balance.

2. The non-linear correction curve g is a power-law function of value $\frac{1}{\gamma}$, and not an arbitrary curve.

3. If, while taking the N differently exposed pictures, there are changes in the gain, white balance or γ values, the pictures will be affected as if the non-linear transform f in equation (2) changed from image to image in the stack.

Let us elaborate a little on this latter point. If an amateur user modifies some settings (other than the exposure time) while taking the pictures, or if she lets the camera work in automatic mode and the camera changes white balance, gain, or gamma value from picture to picture, then the final result of any exposure fusion method that takes these pictures as input will clearly be sub-optimal, as the pictures violate the basic assumption of all exposure fusion models that the only thing changing from one picture to the next is the exposure time. But even in a professional setting we may find out that, although the user has only modified the exposure time from image to image, the camera has, by itself, introduced changes in some of its internal parameters, as the next example illustrates.

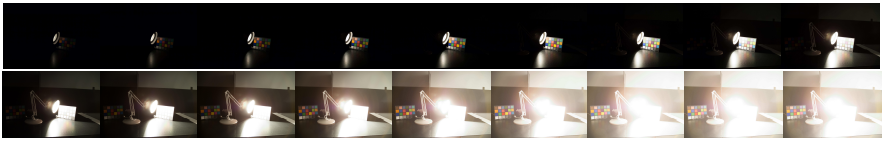

Figure 1: Eighteen individual exposures used by Fairchild in [8] to create the *Luxo Double Checker* HDR image. Figure from [8].

Figure 1 reproduces the 18 individual exposures used by Fairchild in [8] to create the *Luxo Double Checker* HDR image. The images were captured in RAW format, alongside the non-linearly corrected counterparts. For a stack of N RAW pictures R_i the image formation model is:

$$R_i(p) = E(p)\Delta t_i, \quad i = 1,\dots,N, \tag{5}$$

and this equation is valid for the range of luminances for which the sensor operates in the linear range, above the black pedestal and below saturation. This is why, when creating an HDR radiance map through exposure fusion, professional users prefer to take RAW pictures; in this way, there is no need to estimate and invert the CRF that is applied to the non-linearly modified pictures stored in 8 bits per channel form. Applying the logarithm to both sides of equation (5) and leaving only the exposure term on the right we get

$$\log\left(\frac{R_i(p)}{\Delta t_i}\right) = \log(E(p)), \quad i = 1,\dots,N, \tag{6}$$

therefore if we plot $\log\left(\frac{R_i}{\Delta t_i}\right)$ versus $\log(E)$ we should get a single line of slope one. This is indeed approximately the case, as we can see in Figure 2(a). In principle the same could be said in the non-linear case when applying the logarithm to equation (3):

$$\log\left(\frac{g(J_i(p))}{\Delta t_i}\right) = \log(E(p)), \quad i = 1,\ldots,N, \tag{7}$$

because if we plot $\log\left(\frac{g(J_i)}{\Delta t_i}\right)$ versus $\log(E)$ we should also get a single line of slope one. In practice, though, this does not always happen, as Figure 2(b) shows. The fact that the values for $\log\left(\frac{g(J_i)}{\Delta t_i}\right)$ are rather spread implies that it was wrong to assume f (as well as its inverse g) were constant, and therefore the conclusion is that the camera must have modified the values for some of its parameters, α, A, γ, when the exposure time Δt_i is changed. The net result is that HDR radiance maps obtained from exposure fusion of non-linear data may have substantially more error than if computed directly from the linear, RAW data, due to these unwanted modifications.

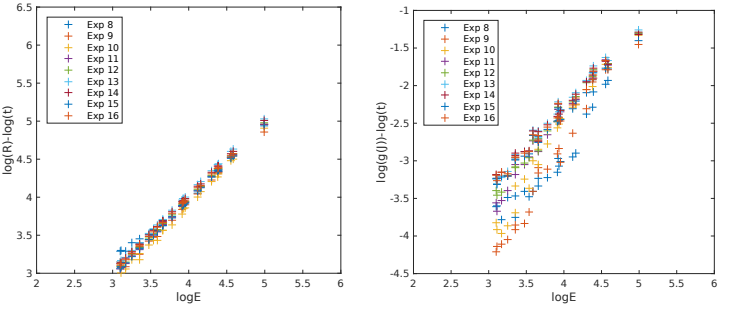

Figure 2: Plots computed for points in the colored squares in the dark color checker in Figure 1, using (a) the RAW values, and (b) the JPEG values. While in both cases the plots should theoretically be a single line of slope one, it can be seen that in the JPEG case the points are more dispersed than in the RAW case.

In this paper we follow the camera color processing pipeline of equation (4) and propose a method to improve exposure fusion, compensating for the aforementioned unwanted changes in gain, color or gamma correction value and allowing us to obtain more precise radiance maps. Our proposed method uniformizes these parameters by matching the gain, color and gamma correction transforms of all pictures to those of a reference picture in the stack, using the framework introduced in [24, 25]. From a set of LDR images we first estimate the gamma correction parameter for each image, then linearize all images (so they become proportional to the radiance), then we select one (the better exposed one) as reference, and color correct all the other images to that reference, and finally we merge all these linearized color corrected images with the linearized reference obtaining our HDR radiance map. Our method is particularly useful in cases where images have been taken by amateur users, allowing automatic camera options such as auto white-balance (AWB) or picture style variation, but also for professional users or researchers that need to work with the different exposures in non-RAW (e.g. JPEG) form and want to reduce the impact of the changes inadvertently introduced by the camera when modifying the exposure time.

Finally, let us also note that although the experiments on this paper deal with static scenes, our method can potentially be extended to more generic situations like non-static

scenes with moving cameras, as the framework used for color and gamma stabilization does not require image registration.

2 Related Work

The creation of a HDR radiance map from a set of LDR images obtained at multiple exposure times is an ongoing research topic [1, 7, 13, 22]. Mann and Picard [16] presented what it is considered the first work on the problem, proposing a parametric method for computing a response function for the camera. Then, LDR images are merged taking into account the derivative of the inverse response. Debevec and Malik [5] used a non-parametric method, under a smoothness constraint, to recover the camera response function (CRF). Once the CRF is computed, the different LDR images are combined into a single HDR image by using a hat weighting function.

Mitsunaga and Nayar [18] presented a method where no precise exposure values were required. In this case, they computed the CRF based on a polynomial model. Tsin *et al*. [23] proposed an iterative method which estimates a non-parametric response function based on a statistical model of CCD imaging process.

All the above mentioned algorithms assume both a fixed camera and a static scene. Less restrictive assumptions where presented in Mann [15] where he used an iterative method to compute the CRF from a set of images with different rotation and zoom. Kim and Pollefeys [11] presented a method to compute point correspondences allowing free movements in the image sequence. Grossberg and Nayar [8] proposed a method based on histograms to relate two images with different exposure times, to avoid spatial correspondences. Hu *et al*. [10] worked on aligning images in a HDR image stack in a non-rigid scene.

More recently, Granados *et al*. [7] proposed a method that simultaneously estimates the irradiance and its uncertainty. The approach is based on the use of the weighting function estimated under the assumption of compound-Gaussian noise. Tocci *et al*. [22] presented an optical architecture for HDR imaging that allows simultaneous capture of high, medium, and low-exposure images on three sensors at high fidelity with efficient use of the available light combined with a HDR merging algorithm. Kronander *et al*. [13] performed the HDR reconstruction directly from the RAW data by fitting local polynomial approximations to observed sensor data and incorporating spatially varying sensor noise. Finally, a deep review and analysis on different methods for HDR generation and their performance bounds was recently performed by Aguerrebere *et al*. [1].

3 Methodology

3.1 Our HDR radiance map generation algorithm

In order to create a HDR radiance map of a scene we need to combine the values captured by the sensor, which are proportional to absolute radiance, which we call $[R,\ G,\ B]_{in}$. However, digital cameras provide us with low dynamic range images with intensity values equal to $[R,\ G,\ B]_{out}$. The typical color processing pipeline can be modeled as in equation (4) and is the composition of linear and nonlinear mappings, where A, a 3×3 matrix, is defined as the set of color operations applied to the radiance, e.g. white balance, color correction,

colorimetric matrix, and the nonlinear mapping is a γ function [2].

Our implementation follows the approach in [24], which performs color stabilization based on the camera color pipeline as defined in equation (4). The main steps of our method are summarizes in Algorithm 1. The input is given as a set of LDR images of different exposures $I_j,\ j = 1,\ldots,N$ of the same HDR static scene. From these input images, we first select the best exposed image $I_{N'}$ as the one with less over and under-exposed pixels. Later, images are registered following [27] to get accurate one-to-one pixel correspondences, then for each $(I_j,\ I_{N'})$ pair we undo the gamma correction and finally we compute the color correction matrix H_j that transforms colors from gamma corrected I_j to gamma corrected $I_{N'}$.

$$\begin{bmatrix} R \\ G \\ B \end{bmatrix}_{out_j} = \left(A_j \cdot \begin{bmatrix} R \\ G \\ B \end{bmatrix}_{in} \right)^{\gamma_j}, \quad \begin{bmatrix} R \\ G \\ B \end{bmatrix}_{out_{N'}} = \left(A_{N'} \cdot \begin{bmatrix} R \\ G \\ B \end{bmatrix}_{in} \right)^{\gamma_{N'}} \tag{8}$$

$$A_{N'} \cdot A_j^{-1} \begin{bmatrix} R \\ G \\ B \end{bmatrix}_{out_j}^{\frac{1}{\gamma_j}} = A_{N'} \cdot \begin{bmatrix} R \\ G \\ B \end{bmatrix}_{in}. \tag{9}$$

Let us note that if we consider the triplet $(R,\ G,\ B)_{in}$ as the sensor exposure, that is, as the irradiance multiplied by the exposure time, we can treat $(R,\ G,\ B)_{in}$ as the irradiance and bring the exposure time information into the matrix A; in this way from equation (8) we get that the linearized computed images $I_j^{'}$ are proportional to the irradiance.

From now on let us call H_j the matrix $A_{N'} \cdot A_j^{-1}$. The computation of $\{\gamma_j, H_j\}$ for all the pairs is done applying [25]. Each matrix H_j is determined by a system of equations based on the direct correspondences between pixels of the image pair, i.e. each pair of corresponding pixels will give us an instance of equation (9). This overdetermined system is solved using the least squares method, discarding over and under-exposed pixels, and we apply the RANSAC method to remove the remaining outliers (notice that in the case of scenes with moving objects we are still able to equalize the colors of all the bracketed images). The new transformed linear images $I_j^{'}$, see Figure 3, are defined as,

$$I_j^{'} = H_j \cdot I_j^{\frac{1}{\gamma_j}}, \text{ for } j = 1,\ldots,N. \tag{10}$$

Then, in the last stage we average these new linear images from equation (10), applying the weighting function described in [4], a trapezoidal function discarding saturated and noisy pixels. Thus, we obtain a HDR radiance map for the best exposure time reference.

4 Experiments

4.1 Fairchild data

We performed our experiments using the Fairchild dataset [6]. The online public-domain database http://rit-mcsl.org/fairchild/HDR.html provides 106 different scenes

[2] We don't consider the non-linearity introduced by clipping output values into the available range, but this shouldn't alter the results in a significant way, as argued in [24].

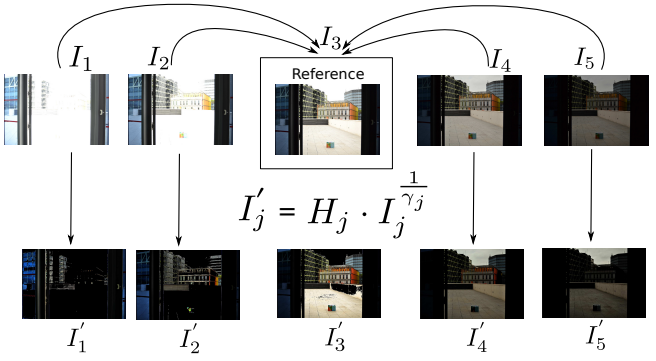

Figure 3: A set of 5 LDR images of a high dynamic range scene: the images I_i, $i = 1,\ldots,5$ are acquired with different exposure times, then the best exposed image, I_3 in this case, is chosen to be the reference image. We compute the new I'_i by applying equation (10) to each of them. Notice that pixels over or under-exposed are not taken into account for the computation and are masked with black in the figure.

Algorithm 1 HDR radiance map generation

Input: set of N images
Result: *HDR* radiance map
1. Select the best exposed image $I_{N'}$,
2. Register the images, [27],
3. For each pair $(I_j,\ I_{N'}),\ j = 1,\ldots,P$, [24]:
  3.1. Undo γ_j correction, and
  3.2. Estimate H_j color correction matrix.
4. Average the new linear images I'_j, [9].

with HDR images in EXR format, along with JPEG versions of all the exposures. It contains as well, for some of the images, colorimetric measurements and color appearance data. Images are acquired using a *Nikon D2x* DSLR camera. For our experiments we randomly selected 18 of these images (10 outdoor, 6 indoor and 2 night scenes): *AirBellowsGap, AmikeusBeaverfDamPM1, DelicateFlowers, Frontier, LabBooth, LabWindow, LabTypWriter, LuxoDoubleChecker, GeneralGrant, CanadianFalls, LittleRiver, LetchWithTeaTable1, DevilsBathTub, WillyDesk, DelicateArch, HancockKitchenOutSide, LasVegasStore* and *JesseBrowns*. The number of LDR images for each HDR one is 9, except for *LuxoDoubleChecker* that has 18. In each scene, the whole dynamic range is covered by the acquired images which are ordered by their exposure time value, and we select the central image as the reference one, with the intention to maximize the number of properly exposed pixels.

4.2 HDR ground truth construction

Let us consider N RAW images obtained by the camera. From the header of the RAW files we read the following parameters: 1) dark and saturation values, which are the minimum and maximum values that the camera gives, 2) a 3×1 array containing the white balance values for each channel and 3) the CFA Bayer pattern, e.g. *'rggb'*. The ground-truth construction

Algorithm 2 Convert RAW HDR image into color

Input: HDR_L
$dark$, $saturation$
$[wb_R, wb_G, wb_B]$
$CFA\ Bayern\ pattern$
Result: HDR_{color}
1. Normalize: linearly scale min of HDR_L to dark value and max to saturation value.
2. Apply white balance ($[wb_R, wb_G, wb_B]$).
3. Demosaic using CFA Bayer pattern.
4. Apply color transformation: multiply each pixel triplet $[R,G,B]$ by 3×3 matrix $M_{color} = E \cdot C$, where E is the matrix converting XYZ values into sRGB values, and C is the sensor characterization matrix that transforms RGB sensor values into standard XYZ values.

is defined in two stages. The first stage is the merging step, where N RAW images with different exposure times Δt_i are combined to obtain a RAW HDR image HDR_L:

$$HDR_L = \frac{\sum_{i=1}^{P} \omega_i (RAW_i / \Delta t_i)}{\sum_{i=1}^{P} \omega_i}, \tag{11}$$

where the weighting function ω_i takes values 0 or 1, by clipping the over and under exposed values (those above 0.92 or below $0.8 \cdot 10^{-3}$). The second stage converts the obtained HDR_L image into color, and it is described in Algorithm 2. For demosaicing we utilize the method proposed by Malvar *et al*. [14].

4.3 Evaluation

In this section we compare the results from our algorithm and the classical approach of Debevec and Malik [5], considering that most recent methods follow the same assumptions: color channels are independent, non-linear correction curves are monotonic and smooth, and the camera response remains constant while changing the exposure times. To this end, for each of the Fairchild images we test on, we compute a ground truth (GT) high dynamic range image, and calculate the Peak Signal to Noise Ratio (PSNR) between GT and the HDR radiance map obtained with our method and that of [5], for the RGB channels as well as for the luminance channel L. In order to perform a fair comparison, firstly we remap both our HDR result and that of Debevec and Malik to the range of the ground truth by linear scaling.

4.3.1 Results

We have computed the results for all the 18 images. We denote the different PSNR errors as $PSNR_i$ where the subscript denotes the red, green, blue, or luminance channel respectively. Results presented as averages for all the images are shown in Table 1. Our method outperforms Debevec and Malik's in each of the four channels, with an improvement ranging between 6% and 11%. We also studied the behaviour of the results in a per-image base, and our method outperforms Debevec and Malik's for 3 or 4 of the channels in more than 75% of the cases. Qualitative results of our approach are presented in Figure 4, where both the HDR output of Debevec and Malik and our approach are illustrated (after the same tone-mapping [19] has been applied to both of them). In particular, we want to focus the reader to the fact that in our results more contrast, and therefore, more details are perceived.

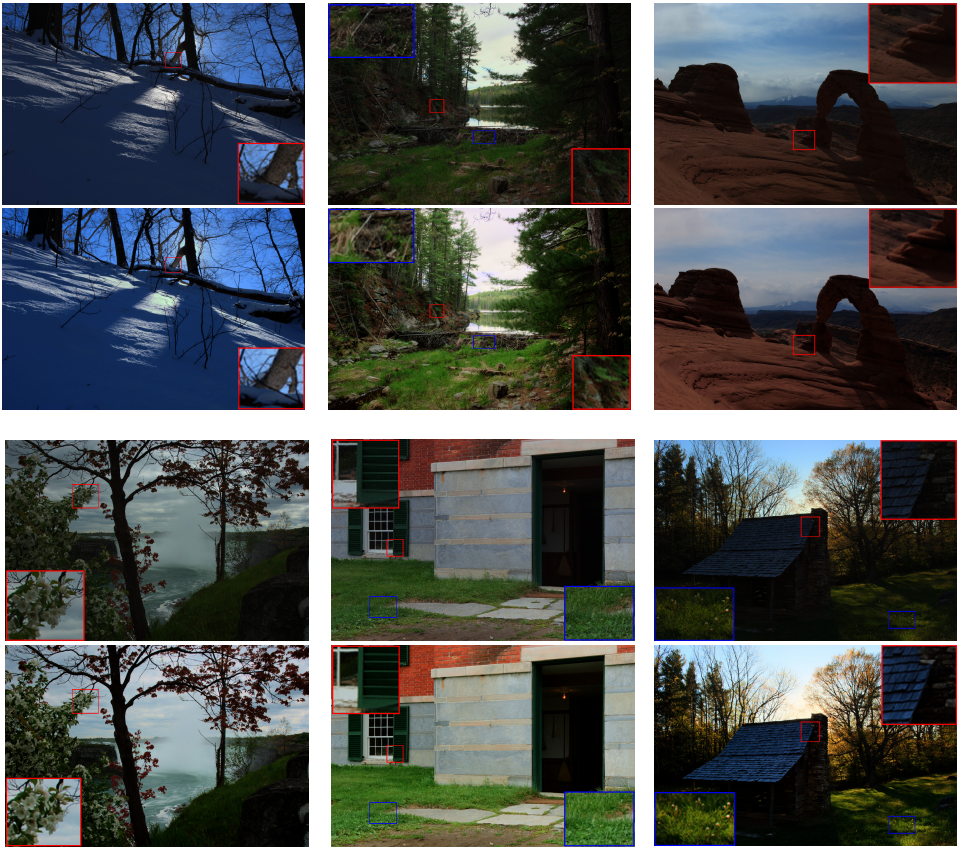

Figure 4: HDR results (tone mapped with [20]) obtained with the method of Debevec and Malik (1st and 3rd rows) and with the proposed approach (2nd and 4th rows).

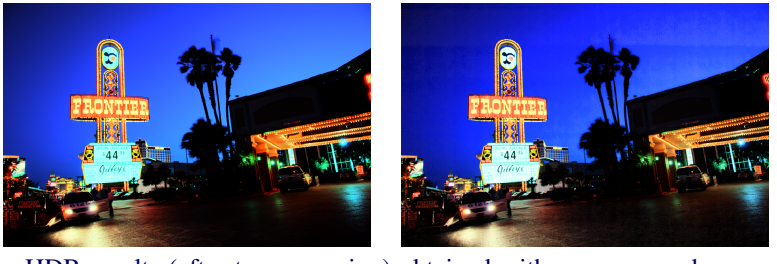

Figure 5: HDR results (after tone mapping) obtained with our proposed approach. Left: taking as reference the 5th image. Right: reference is the 7th image.

Finally, Figure 5 shows a current limitation of our method, which is its dependence on the particular image that has been chosen as reference. On the left we see the result (after the same tone mapping is applied) when choosing the 5th image as reference, while on the right the result is based on the 7th image as the reference. The differences are more noticeable for artificial surfaces with highly saturated colors.

Table 1: Average, over the 18 Fairchild images used, of the PSNR on the color channels (R,G,B) and the luminance channel (L), for the method of Devebec and Malik [5] and the proposed approach.

	$PSNR_R$	$PSNR_G$	$PSNR_B$	$PSNR_L$
Devebec and Malik [5]	25.70	26.15	26.80	26.30
Proposed	**28.47**	**28.73**	**28.37**	**28.86**

5 Conclusion

In this paper we have presented an algorithm to obtain an HDR map from a set of LDR images which is based upon the digital camera imaging pipeline. Results show that our algorithm quantitatively outperforms the work of Debevec and Malik in most of the cases considered. Let us also note that, as stated during the paper, our algorithm can be integrated into HDR methods that handle dynamic scenes, since it does just require a discrete set of point correspondences [25]. We are currently working on making the proposed method more robust to changes in the selection of the reference image, and also on extending the results using all the 106 scenes from Fairchild dataset.

Acknowledgements

This work was supported by the European Research Council, Starting Grant ref. 306337, by the Spanish government, grant ref. TIN2012-38112, and by the Icrea Academia Award. We would like to thank Mark Fairchild for providing us with the RAW and JPEG sets of images from his 'HDR Photographic Survey' for evaluation results.

References

[1] C. Aguerrebere, J. Delon, Y. Gousseau, and P. Musé. Best Algorithms for HDR Image Generation. A Study of Performance Bounds. *SIAM Journal on Imaging Sciences*, 7 (1):1–34, 2014.

[2] M. Bertalmío. *Image Processing for Cinema*. Chapman & Hall/CRC Mathematical and Computational Imaging Sciences Series. CRC Press - Taylor & Francis, 1st edition, 2014.

[3] S. Bianco, A. Bruna, F. Naccari, and R. Schettini. Color space transformations for digital photography exploiting information about the illuminant estimation process. *JOSA A*, 29(3):374–384, 2012.

[4] B. Bringier, A. Bony, and M. Khoudeir. Evidence Theory for High Dynamic Range Reconstruction with Linear Digital Cameras. *Computer Vision and Image Understanding*, 2014.

[5] P. E. Debevec and J. Malik. Recovering High Dynamic Range Radiance Maps from Photographs. In *Proceedings of the 24th Annual Conference on Computer Graphics and Interactive Techniques*, SIGGRAPH '97, pages 369–378, New York, NY, USA, 1997.

[6] M. D Fairchild. The HDR photographic survey. *Color and Imaging Conference*, 2007 (1):233–238, 2007.

[7] M. Granados, B. Ajdin, M. Wand, C. Theobalt, H.-P. Seidel, and H. Lensch. Optimal HDR reconstruction with linear digital cameras. In *Computer Vision and Pattern Recognition (CVPR), 2010 IEEE Conference on*, pages 215–222, June 2010.

[8] M. D. Grossberg and S. K. Nayar. High Dynamic Range from Multiple Images: Which Exposures to Combine. In *in Proc. ICCV Workshop on Color and Photometric Methods in Computer Vision (CPMCV)*, 2003.

[9] B. Guthier, S. Kopf, M. Wichtlhuber, and W. Effelsberg. Parallel implementation of a real-time high dynamic range video system. *Integr. Comput.-Aided Eng.*, 21(2):189–202, April 2014.

[10] J. Hu, O. Gallo, K. Pulli, and X. Sun. HDR Deghosting: How to deal with Saturation ? In *CVPR*, 2013.

[11] S. J. Kim and M. Pollefeys. Robust Radiometric Calibration and Vignetting Correction. *Pattern Analysis and Machine Intelligence, IEEE Transactions on*, 30(4):562–576, April 2008.

[12] J. Kronander, S. Gustavson, and J. Unger. Real-time HDR Video Reconstruction for Multi-sensor Systems. In *ACM SIGGRAPH 2012 Posters*, SIGGRAPH '12, pages 65:1–65:1, New York, NY, USA, 2012. ACM.

[13] J. Kronander, S. Gustavson, G. Bonnet, and J. Unger. Unified HDR reconstruction from raw CFA data. In *Computational Photography (ICCP), 2013 IEEE International Conference on*, pages 1–9, April 2013.

[14] H. S. Malvar, L. He, and R. Cutler. High-quality linear interpolation for demosaicing of bayer-patterned color images. In *Proceedings of the IEEE International Conference on Speech, Acoustics, and Signal Processing*, 2004.

[15] S. Mann. Comparametric equations with practical applications in quantigraphic image processing. *Image Processing, IEEE Transactions on*, 9(8):1389–1406, Aug 2000.

[16] S. Mann and R. W. Picard. On Being 'undigital' With Digital Cameras: Extending Dynamic Range By Combining Differently Exposed Pictures. In *Proceedings of IS&T*, pages 442–448, 1995.

[17] J.J. McCann and A. Rizzi. *The Art and Science of HDR Imaging*. The Wiley-IS&T Series in Imaging Science and Technology. Wiley, 2011.

[18] T. Mitsunaga and S.K. Nayar. Radiometric self calibration. In *Computer Vision and Pattern Recognition, 1999. IEEE Computer Society Conference on.*, volume 1, pages –380 Vol. 1, 1999.

[19] E. Reinhard and K. Devlin. Dynamic range reduction inspired by photoreceptor physiology. *IEEE Transactions on Visualization and Computer Graphics*, 11(1):13–24, 2005.

[20] E. Reinhard, M. Stark, P. Shirley, and J. Ferwerda. Photographic tone reproduction for digital images. *ACM Trans. Graph.*, 21(3):267–276, July 2002.

[21] E. Reinhard, G. Ward, S. Pattanaik, and P. Debevec. *High Dynamic Range Imaging: Acquisition, Display, and Image-Based Lighting (The Morgan Kaufmann Series in Computer Graphics)*. Morgan Kaufmann Publishers Inc., San Francisco, CA, USA, 2005.

[22] M. D. Tocci, C. Kiser, N. Tocci, and P. Sen. A Versatile HDR Video Production System. *ACM Trans. Graph.*, 30(4):41:1–41:10, July 2011.

[23] Y. Tsin, V. Ramesh, and T. Kanade. Statistical calibration of CCD imaging process. In *Computer Vision, 2001. ICCV 2001. Proceedings. Eighth IEEE International Conference on*, volume 1, pages 480–487 vol.1, 2001.

[24] J. Vazquez-Corral and M. Bertalmío. Color Stabilization Along Time and Across Shots of the Same Scene, for One or Several Cameras of Unknown Specifications. *Image Processing, IEEE Transactions on*, 23(10):4564–4575, Oct 2014.

[25] J. Vazquez-Corral and M. Bertalmío. Simultaneous blind gamma estimation. *IEEE Signal Process. Lett.*, 22(9):1316–1320, 2015.

[26] J. Vazquez-Corral, D. Connah, and M. Bertalmío. Perceptual color characterization of cameras. *Sensors*, 14(12):23205–23229, 2014.

[27] G. Ward. Fast, Robust Image Registration for Compositing High Dynamic Range Photographs from Handheld Exposures. *JOURNAL OF GRAPHICS TOOLS*, 8:17–30, 2003.